International Communications in Heat and Mass Transfer 137 (2022) 106236

Contents lists available at ScienceDirect

International Communications in Heat and Mass Transfer

journal homepage: www.elsevier.com/locate/ichmt

Double-diffusive natural convection energy transfer in magnetically influenced Casson fluid flow in trapezoidal enclosure with fillets

Hasan Shahzad [a], Qurrat Ul Ain [b,c], Amjad Ali Pasha [d], Kashif Irshad [e,f], Imtiaz Ali Shah [c], Abuzar Ghaffari [g], Muhammad Bilal Hafeez [h,*], Marek Krawczuk [h]

[a] Faculty of Materials and Manufacturing, College of Mechanical Engineering and Applied Electronics Technology, Beijing University of Technology, 100124, China
[b] Women university of Azad Jammu and Kashmir, Bagh, Pakistan
[c] Department of Mathematics, Air University, PAF Complex E-9, Islamabad 44000, Pakistan
[d] Aerospace Engineering Department, King Abdulaziz University, Jeddah 21589, Saudi Arabia
[e] Interdisciplinary Research Center for Renewable Energy and Power Systems (IRC-REPS), King Fahd University of Petroleum and Minerals, Dhahran 31261, Saudi Arabia
[f] Researcher at K.A.CARE Energy Research & Innovation Center at Dhahran, 31261, Saudi Arabia
[g] Department of Mathematics, Division of Science and Technology, University of Education, Lahore 54770, Pakistan
[h] Gdansk University of Technology, Faculty of Mechanical Engineering and Ship Technology, Institute of Mechanics and Machine Design, Narutowicza 11/12, 80-233 Gdańsk, Poland

ARTICLE INFO

Keywords:
Casson fluid
Trapezoidal fillet cavity
Double diffusive
Inclined magnetic field
FEM

ABSTRACT

The prime motive of this disquisition is to deal with mathematical analysis of natural convection energy transport driven by combined buoyancy effects of thermal and solutal diffusion in a trapezoidal enclosure. Casson fluid rheological constitutive model depicting attributes of viscoelastic liquids is envisioned. The influence of the inclined magnetic field governed by Lorentz field law is also considered. To raise the essence of the presently used computational and physical domain, an innovative structural design called fillet is capitalized at the edges of the cavity. A numerical solution of the leading formulation is sought through Galerkin finite element discretization. Momentum, temperature, and concentration equations are interpolated by quadratic polynomials, whereas pressure distribution is approximated by a linear interpolating function. Domain discretized version is evaluated in view of triangular and rectangular elements. Newton's scheme is employed to resolve the non-linearly discretized system and a matrix factorization-based non-linear solver renowned as PARADISO is used. Validation of results is ascertained by forming an agreement with existing studies. Streamlines, isothermal and iso concentration contours patterns are portrayed to evaluate variation inflow distributions. Kinetic energy, local heat, and mass fluxes are also divulged in graphical and tabular formats.

1. Introduction

Concurrent heat and mass transfer have a common manifestation in nature and yet many industrial settings. Double-diffusive convection refers to fluid flows that are created because of a combination of temperature and concentration gradients. Double-Diffusion convection (D.D·C.) can be found in various scientific domains, including astrophysics, astrophysics and biology, as well as many technical applications, natural gas storage tanks, including many technical applications solar ponds, crystal fabrication, and food processing. Some significant foundational literature, such as Turner et al. [1–3], can help you better to understand this phenomenon. Industrial and geophysical uses of double-diffusive natural convection in enclosures include pollutant dispersions in soil and subsurface water, petrochemical processes, heat exchanger design, fuel cells, thermo-protection systems, and channel type solar energy collectors. As a result, natural convection heat and mass transfer properties are critical.

A lot of experimental, analytical, and numerical research has been conducted in recent years to investigate such remarkable phenomena in distinct insertions. Ostrach et al. [4,5] reported comprehensive analyses on the topic. Gebhart et al. [6] was one of the first to use numerical methods to investigate D.D.C for the vertical flow of laminar fluid in

* Corresponding author.
E-mail addresses: aapasha@kau.edu.sa (A.A. Pasha), kashif.irshad@kfupm.edu.sa (K. Irshad), imtiaz@students.au.edu.pk (I.A. Shah), abuzar.ghaffari@ue.edu.pk (A. Ghaffari), muhammad.bilal.hafeez@pg.edu.pl (M.B. Hafeez), marek.krawczuk@pg.edu.pl (M. Krawczuk).

https://doi.org/10.1016/j.icheatmasstransfer.2022.106236

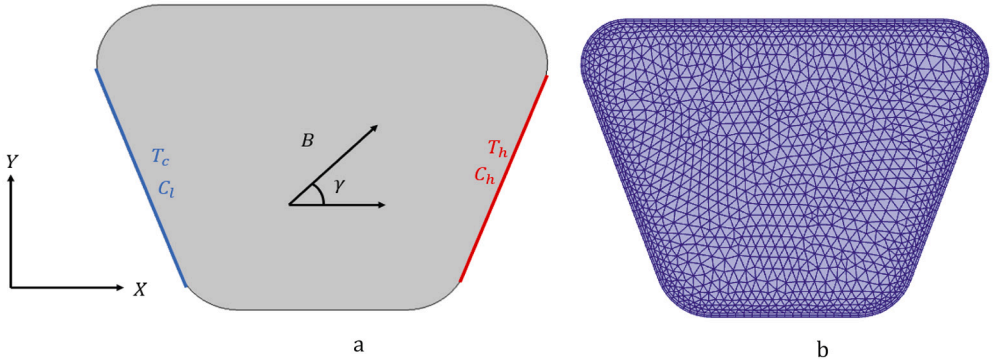

Fig. 1. Diagrammatic representation of the problem.

plumes or over surfaces. This research concentrated on the effects of non-dimensional factors on procedures of double-diffusion on heat and mass transport, as well as the turbulence transition. Scale analysis of heat and mass movement inside the cavities subjected to horizontal temperature and concentration gradients was key research by Bejan [7]. Fundamentally thermal convection, merely solutal convection, heat transfer induced flows, and mass transport induced flows have all been taken into consideration. In partially heated cavities, Mobedi et al. investigated in [8,9] double-diffusive convection. The flow, heat, and mass transfer are numerically investigated by Nikbakhti and Rahimi [10], considering a rectangular-shaped cavity with walls that are partially heated. They discovered that when the heated area is at the bottom, and the cool section is at the top, the transfer of heat and mass is at its highest. [11] Studied the mass and heat transport of Non-Newtonian nanofluid through a porous media. According to their findings, the thickness of the boundary layer decreases as the heat factor and slip parameter increase. [12] Performed the comparative study of different nanoparticles over an exponentially accelerated Riga plate surface. They found that the density of cupric nanofluid is increased by increasing the volume fraction of nanoparticles over Al_2O_3 nanofluid through a decline in velocity distribution. Numerical calculations were performed by [13] to examine the mixed convection in an open trapezoidal cavity. They studied the impact of Reynolds number and Richardson number on various lid-driven sidewall cases. [14] Numerically investigated thermal transport and buoyant convection of $Cu - H_2O$ Nano fluid in an annulus through a thin baffle. The results for different ranges of baffle positions and length was calculated. They discovered when the baffle length is 20% of annular width placed at 80% of the annular height yielded higher thermal transport rates as compared to other length and positions of the baffle. Due to its effect on the electrical conductivity of fluids [15], a magnetic field has been utilized to increase the heat transfer rate in various investigations. A body force known as the Lorentz force [16–21], also known as magneto-hydrodynamic convection heat transfer, influenced flow and heat transfer in this state (MHD). MHD research has become increasingly popular among scholars in recent years [22,23]. Mansour et al. [24] examined natural convection in a cavity with localized energy sources. Concluded that increasing the Rayleigh number and the number of copper oxide nanoparticles increased the Nusselt number, regardless of the cavity's AR. Using the lattice-Boltzmann approach, Mliki et al. [25] studied the natural convective heat transmission nanofluid inside an L-shaped cavity numerically (LBM). They discovered that boosting the Rayleigh number resulted in a rise in the average Nusselt number.

Melt spinning, solar panelling drying, coating innovations, hydraulic pumps, chips used in computers, molten metals, heat dissipation fins, filtration processes, hydrothermal reservoirs, nuclear waste storage, liquefaction gases, casting solidification, and development of biofilm are all examples of natural convection. Researchers have carried out analyses due to their high practical importance. Turan et al. [26] used the power-law model to create natural convection using sidewalls heated partially of an inclusion filled entirely with a non-linear fluid. Ternik and Rudolf [27] used the finite volume approach to simulate thermal and hydrodynamic forces for a power-law model along with a Boussinesq approximation. Sajoudi et al. [28], in a container of trapezoidal shape flooded with passive power-law fluid, defined convection by maintaining the surface adiabatically. Turan et al. [29] investigated the effect of heaters positioned just on the boundaries of an enclosure of rectangular shape on laminar, time-independent, and natural convection flow. The evaluation for heat transfer variance against the Prandtl number is done by Ternik and Buchmiester [30]. They discovered the buoyantly generated flow in a square shaped enclosure with Dirichlet heat flux circumstances of power-law fluid. Alloui and Vesseur [31] studied convective heat transport in a non-linear fluid contained in a container in the vertical direction by using.

Materials with differing viscosities react differently to stressors. The contrasts in behavior between Newtonian and non-Newtonian liquids separate them. Non-Newtonian fluids have non-linear properties, while Newtonian fluids have linear strains vs. stress factors. Non-Newtonian liquid applications include cooling systems, oil-pipeline friction, flow traces, surfactants, lubrication, mining, slurries, and biomedical flows. Non-Newtonian liquids are separated into two groups: shear thickening and thinning liquids, for a complete analysis. Non-Newtonian fluids have become increasingly significant in modern processes such as oil refining, food manufacturing, cooling, and heating systems, polymerization, nuclear power plants, flow tracing, reduction of friction, and so on. Numerous models have been proposed by rheological experts to portray the categorization in this regard. Many non-Newtonian fluid models have been proposed to define these difficult natural phenomena considering the above explanation and industrial application of non-Newtonian materials. Casson (1995) introduced the Casson fluid model, which he observed does not follow Newton's viscosity law. Blood and chocolate flows, for example, are found to become less effective for interpreting rheological facts than the aforesaid model. The full investigation of Casson fluid through various impacts has been considered, including references in [32–36].

According to a review of the aforementioned scientific research, the diffusion phenomenon in non-Newtonian liquid caused by thermal and solutal buoyancy driven forces has not yet been investigated. Furthermore, despite the overwhelming rise of magnetic fields in various modern engineering systems, such features are seldom examined together. As a result, the focus of this endeavor is on filling this gap by inserting Casson non-Newtonian liquid with isothermal and iso-concentration limitations on the cavity's right wall. To do this, the mathematical definition of the problem is modelled as a partial differential expression, and then similarity variables are employed to convert PDEs to ODEs. Simulation with a finite element methodology is used to carry out the numerical solution of the formulated problem. Finally, the effects of important parameters on related distributions are depicted in a

Table 1
Grid convergence study for the mean Nusselt, Sherwood number, and kinetic energy for $\beta = 1$, $Ha = 25$, $Le = 2.5$, $Pr = 6.8$, *and* $Ra = 10^5$.

Grid	*NEL*	*DOFs*	Nu_{avg}	Sh_{avg}	K.E.
L_1	258	1795	0.19038	1.3207	106.11
L_2	432	2950	0.15949	1.2643	104.50
L_3	668	4361	0.14190	1.2374	101.93
L_4	1156	7394	0.12585	1.2193	100.29
L_5	1758	10,991	0.10647	1.1934	99.614
L_6	2876	17,459	0.094493	1.1768	98.738
L_7	7288	43,529	0.066337	1.1389	97.899
L_8	18,206	106,801	0.047210	1.1125	97.518
L_9	29,164	167,070	0.047164	1.1125	97.408

Table 2
Comparison of the average Nusselt number at the bottom wall between the present solution and that of Shafqat et al. [39] for $Ha = 25$, Le, 2.5, $Pr = 6.8$, $Ra = 10^5$ and different values of β.

β	[39]	Present
0.1	2.38986	2.39023
1	3.81194	3.81168
5	4.27587	4.27511
10	4.35556	4.35470

graphical and tabular format.

The present work is systematized in the following manner: The geometrical and mathematical description of investigation are presented in Section 2. The adopted computational scheme is presented in section 3. The obtained results are explained and discussed by plotting various graphs in Section 4. Some engineering based quantities are discussed in Section 5. The work is finally concluded in last section.

2. Mathematical model

2.1. Problem description

Let us consider a 2-dimensional, steady-state, uniform, incompressible and laminar flow of Casson fluid enclosed in a trapezoidal fillet cavity. The right cavity wall is heated at a fixed temperature (T_h) with a high concentration (C_h), whereas the left cavity wall is under the influence of cooling temperature (T_c) with low concentration (C_l), where ($T_h > T_c$) and ($C_h > C_l$). The remaining parts of the cavity are supposed to be adiabatic. The magnetic field at an angle of γ to the horizontal direction with a strength of B was applied. The unstructured mesh is used to discrete the equations all over the cavity. The flow problem and unstructured mesh schematic geometry are shown in Fig. 1a and Fig. 1b, respectively.

2.2. Governing equations

The continuity, momentum, energy, and concentration equations are presented as follows, predicated on the assumption indicated above:

$$\frac{\partial u^*}{\partial x^*}+\frac{\partial v^*}{\partial y^*}=0, \tag{1}$$

$$\rho\left(u^*\frac{\partial u^*}{\partial x^*}+v^*\frac{\partial u^*}{\partial y^*}\right)=-\frac{\partial p^*}{\partial x^*}+\mu\left(1+\frac{1}{\beta}\right)\left(\frac{\partial^2 u^*}{\partial x^{*2}}+\frac{\partial^2 u^*}{\partial y^{*2}}\right)+\Lambda_{x^*}, \tag{2}$$

$$\rho\left(u^*\frac{\partial v^*}{\partial x^*}+v^*\frac{\partial v^*}{\partial y^*}\right)=-\frac{\partial p^*}{\partial x^*}+\mu\left(1+\frac{1}{\beta}\right)\left(\frac{\partial^2 v^*}{\partial x^{*2}}+\frac{\partial^2 v^*}{\partial y^{*2}}\right)+\Lambda_{y^*}, \tag{3}$$

$$u^*\frac{\partial T}{\partial x^*}+v^*\frac{\partial T}{\partial y^*}=\alpha_e\left(\frac{\partial^2 T}{\partial x^{*2}}+\frac{\partial^2 T}{\partial y^{*2}}\right) \tag{4}$$

$$u^*\frac{\partial c}{\partial x^*}+v^*\frac{\partial c}{\partial y^*}=D\left(\frac{\partial^2 c}{\partial x^{*2}}+\frac{\partial^2 c}{\partial x^{*2}}\right) \tag{5}$$

where ρ, μ, β, α_e, D are fluid density, kinematic viscosity, Casson parameter, thermal diffusivity, diffusion coefficient and $\Lambda = (\Lambda_{x^*}, \Lambda y^*)$ are the force index owing to magnetic field and the Boussinesq approximation defined as follows,

$$\Lambda_{x^*}=\sigma B_0^2\left(v^* sin\gamma cos\gamma - u^* sin^2\gamma\right) \tag{6}$$

$$\Lambda_{y^*}=\sigma B_0^2\left(u^* sin\gamma cos\gamma - v^* cos^2\gamma\right)+\rho g[\beta_T(T-T_c)+\beta_c(c-c_c)] \tag{7}$$

where β_c and β_T show the solutal and the thermal expansions, respectively.

2.3. Boundary conditions

$$u^*=0, v^*=0, T=T_h, c=c_h, \text{(for hot side)}$$

$$u^*=0, v^*=0, T=T_c, c=c_c, \text{(for cold side)}$$

$$u^*=0, v^*=0, \frac{\partial T}{\partial n}=\frac{\partial c}{\partial n}=0.\text{(rest of the wall)} \tag{8}$$

where n indicates the normal vector on the boundary.

The dimensionless parameters are used to convert the dimensional Eqs. (1 − 7) and the boundary condition (8) to non-dimensional form.

$$(X^*,Y^*)=\frac{(x^*,y^*)}{L},(U^*,V^*)=\frac{(u^*,v^*)L}{\alpha},P^*=\frac{p^*L^2}{\rho\alpha^2},\theta^*=\frac{T-T_c}{T_h-T_c},C^*=\frac{c-c_c}{c_h-c_c} \tag{9}$$

$$\alpha_e=\frac{k_e}{(\rho c_p)_f},Ra=\frac{\rho^2\beta_T g L^3\Delta TPr}{\upsilon^2},Le=\frac{\alpha_e}{\mathrm{D}},Ha=BL\sqrt{\frac{\sigma}{\mu}},Pr=\frac{\nu}{\alpha}. \tag{10}$$

The non-dimensional system with boundary conditions is constructed by substituting Eqs. (9 − 10) in (1 − 5) and (7 − 8) is as follows:

$$\frac{\partial U^*}{\partial X^*}+\frac{\partial V^*}{\partial Y^*}=0 \tag{11}$$

$$\left(U^*\frac{\partial U^*}{\partial X^*}+V^*\frac{\partial U^*}{\partial Y^*}\right)=-\frac{\partial P^*}{\partial X^*}+Pr\left(1+\frac{1}{\beta}\right)\left(\frac{\partial U^*}{\partial X^*}+\frac{\partial U^*}{\partial Y^*}\right)+\Lambda_{X^*} \tag{12}$$

$$\left(U^*\frac{\partial V^*}{\partial X^*}+V^*\frac{\partial V^*}{\partial Y^*}\right)=-\frac{\partial P^*}{\partial Y^*}+Pr\left(1+\frac{1}{\beta}\right)\left(\frac{\partial V^*}{\partial X^*}+\frac{\partial V^*}{\partial Y^*}\right)+\Lambda_{Y^*} \tag{13}$$

$$U^*\frac{\partial\theta^*}{\partial X^*}+V^*\frac{\partial\theta^*}{\partial Y^*}=\frac{\partial^2\theta^*}{\partial X^{*2}}+\frac{\partial^2\theta^*}{\partial Y^{*2}} \tag{14}$$

$$U^*\frac{\partial C^*}{\partial X^*}+V^*\frac{\partial C^*}{\partial Y^*}=\frac{1}{Le}\left(\frac{\partial^2 C^*}{\partial X^{*2}}+\frac{\partial^2 C^*}{\partial Y^{*2}}\right) \tag{15}$$

where

$$\Lambda_{X^*}=PrHa^2\left(V^* sin\gamma cos\gamma - U^* sin^2\gamma\right), \tag{16}$$

$$\Lambda_{Y^*}=PrHa^2\left(U^* sin\gamma cos\gamma - V^* cos^2\gamma\right)+RaPr(\theta^*+NC^*). \tag{17}$$

Here are dimensionless boundary conditions:

$$U^*=0, V^*=0, \theta^*=1, C^*=1.\text{(for hot side)} \tag{18}$$

$$U^*=0, V^*=0, \theta^*=0, C^*=0.\text{(for cold side)} \tag{19}$$

$$U^*=0, V^*=0, \frac{\partial\theta^*}{\partial n}=\frac{\partial C^*}{\partial n}=0.\text{(for rest of the walls)} \tag{20}$$

On the hot wall, the local and mean Nusselt number, local and mean

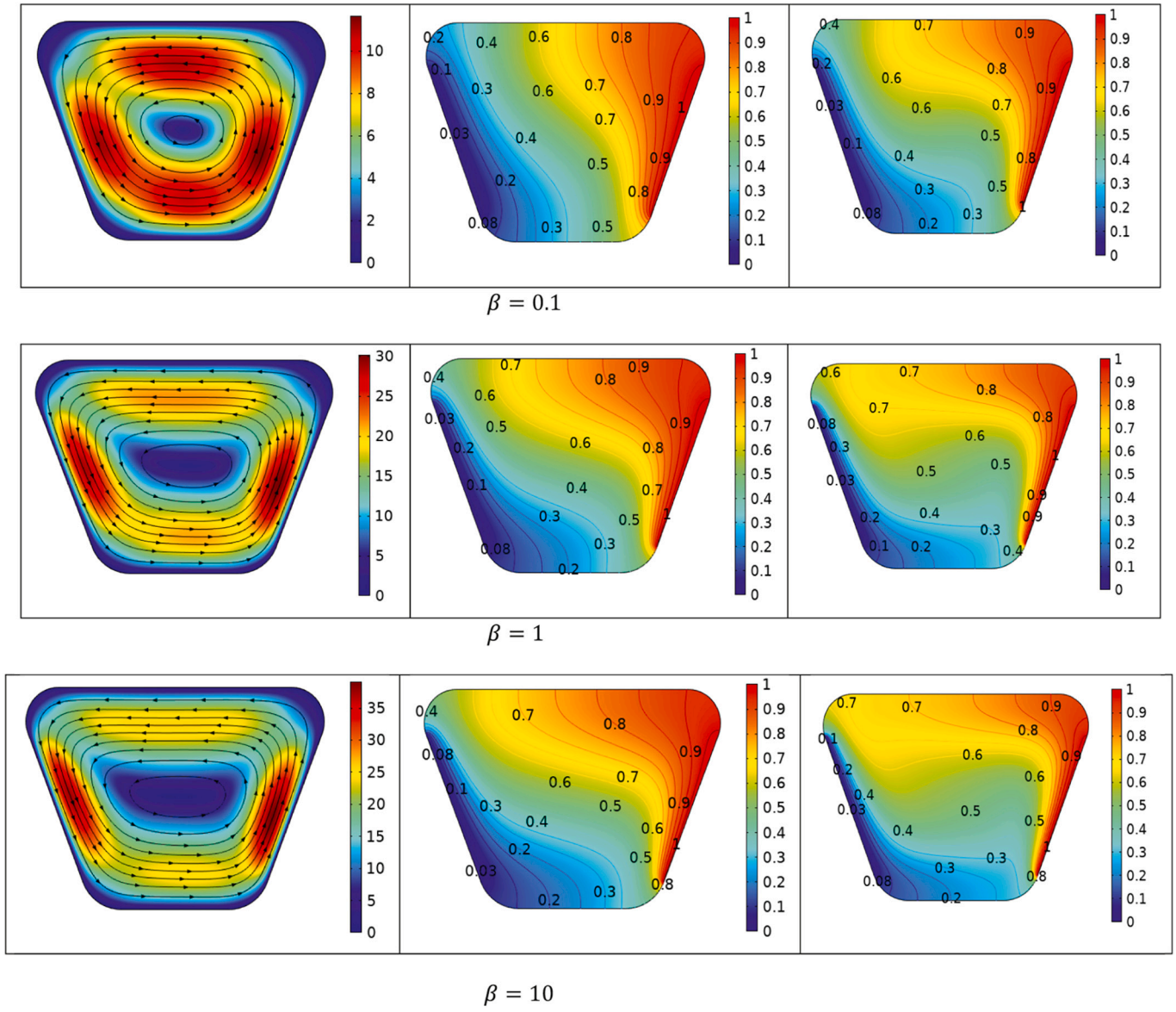

Fig. 2. Variation in velocity, temperature, and concentration profile against Casson parameter (β).

Sherwood number, are calculated by,

$$Nu = \left(-\frac{\partial \theta^*}{\partial X^*} \right)_{X^*=0} \tag{21}$$

$$Sh = \left(-\frac{\partial C^*}{\partial X^*} \right)_{X^*=0} \tag{22}$$

$$Nu_{avg} = \int_0^1 Nu \, dY^* \tag{23}$$

$$Sh_{avg} = \int_0^1 Sh \, dY^* \tag{24}$$

Additionally, the quantities above, the computation and examination of a global quantity is also interesting, named total kinetic energy and is defined as,

$$K.E = \frac{1}{2}\int_\Omega \|U\|^2 \, d\Omega \tag{25}$$

where $U = (U^*, V^*)$ is the velocity vector.

3. Solution methodology

Lots of computational methodologies were used for studying fluid flow and heat transfer inside enclosures and cavities [37]. The discretization is done by the finite element method FEM used for solving the governing Eqs. (11 − 15) with the boundary conditions Eqs. (18 − 20) using the finite-element methodology [38]. The Newtons method is used to linearize the resulting discrete system of nonlinear equations. After guaranteeing a particular threshold factor of tolerance, the iterative method for nonlinearity is terminated.

3.1. Grid convergence

To demonstrate the efficacy of the attained outcomes, multiple grids have been employed when $Ha = 25$, $Ra = 10^5$, $Pr = 6.8$, $Le = 2.5$ *and* $\beta = 1$ and are shown in Table 1. As a result, the number of degrees of freedom (DOFs) and the Inumber of elements (NEL) range from 1795 to 167,070 and 258 to 29,164, respectively. For the last two grids (L_8 and L_9), the difference between the Nusselt and Sherwood numbers is negligible. Hence, DOFs of 106,801 and NEL of 18,206 can provide gird independence, and using them the numerical results are presented. The

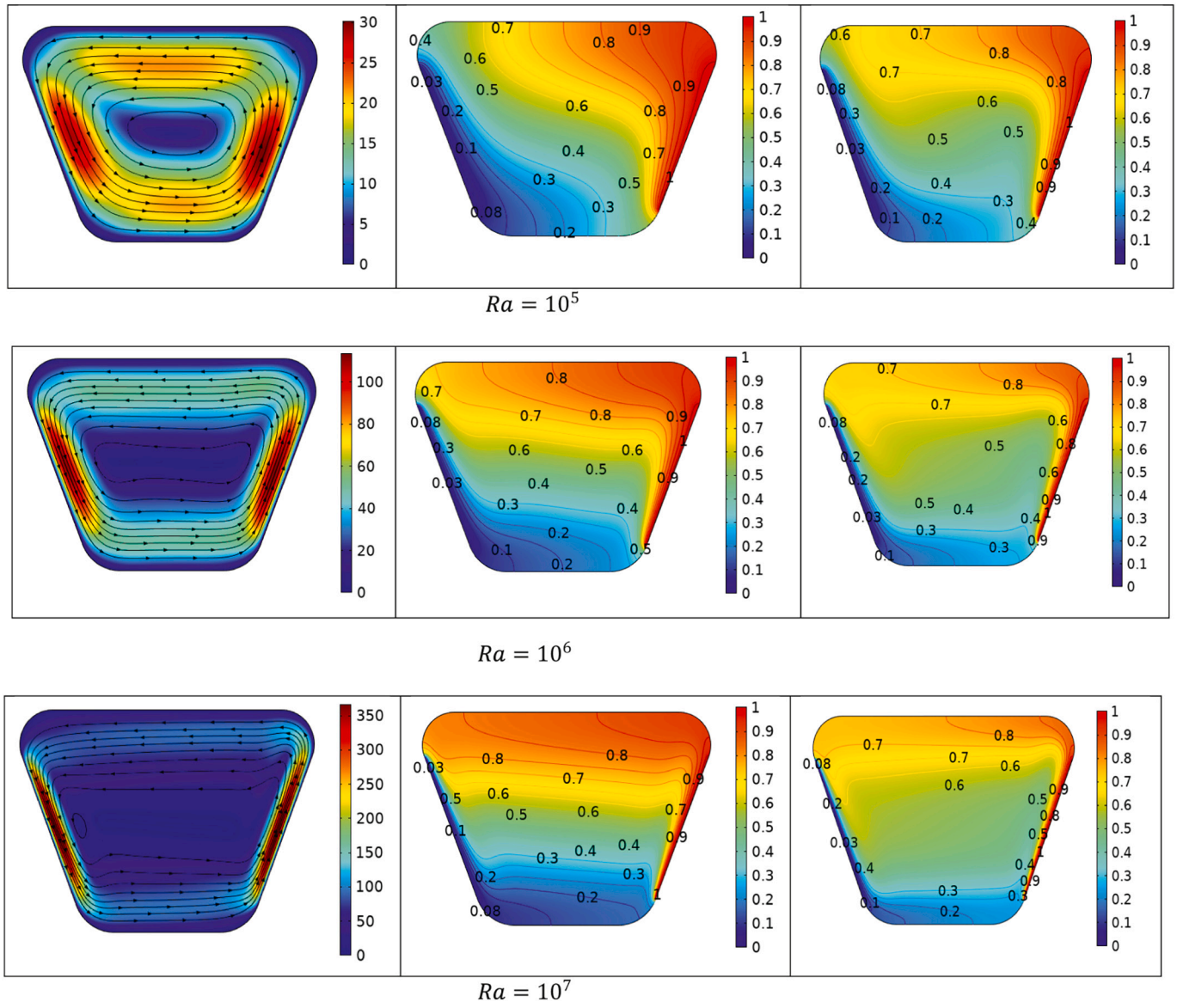

Fig. 3. Variation in velocity, temperature and concentration profile against Rayleigh number (*Ra*).

size of mesh for the present study is revealed in the following Fig. 1b.

3.2. Code validation

Once grid independence is established, the validation of code is presented iagainst the results of Shafqat et al. [39] for the average Nusselt number by fixing $Ha = 25$, Le, 2.5, $Pr = 6.8$, $Ra = 10^5$ and different values of β shown in Table 2. The comparison demonstrated the accuracy of our results, and a good agreement among the respective results is obtained, which ensures that the results obtained for the present study are reliable for accuracy check.

4. Result and discussion

This portion is presented to interpret attained results in the form of streamlines, isotherms and isoconcentration distributions against a wide range of involved physical parameters like Casson parameter (β), Hartmann number (*Ha*), Rayleigh number (*Ra*), and Lewis number (*Le*). Subsequently, global, and local quantities of interest like mass flux coefficient (Sherwood number), heat flux coefficient (Nusselt number), and kinetic energy are computed..

The impression of Casson parameter (β) on velocity, temperature, and concentration fields is exhibited in Fig. 2. Here, (β) is varied from 0.1 to 10, and other parameters like $Pr = 6.8$, $Ha = 25$, $Ra = 10^5$, $Le = 2.5$, $N = 1$, $\gamma = 30^{\circ}$ are fixed. The fluid rotates clockwise due to the high temperature of the right wall and the low temperature of the left wall. The double-diffusive conventional heat transfer of the enclosure are responsible for the isotherms and isoconcentration patterns. Variation in temperature distribution against Casson fluid parameter (β) is also evaluated in Fig. 2. It is seen from the sketches that at (β) = 10 magnitudes of isotherms attained greater values because at a higher magnitude of β, velocity of fluid increases. Thus, as an outcome, average kinetic energy elevates, and the temperature profile shows incrementing trend. The isoconcentration pattern do not change significantly as the Casson parameters increase..

Fig. 3 illustrates the change in magnitude of streamlines, isotherms, Isoconcentration against (*Ra*), ranging from $Ra = 10^5 - 10^7$ and by fixing $Pr = 6.8$, $Ha = 25$, $\beta = 1$, $Le = 2.5$, $N = 1$, $\gamma = 30^{\circ}$. The streamlines move closer to the walls as the Rayleigh number increases, and the horizontal and parallel isotherms and isoconcentration.

In Fig. 4 we investigated the effect of $Le = 0.1 - 10$ on momentum, temperature, and concentration distributions. No significant changes in

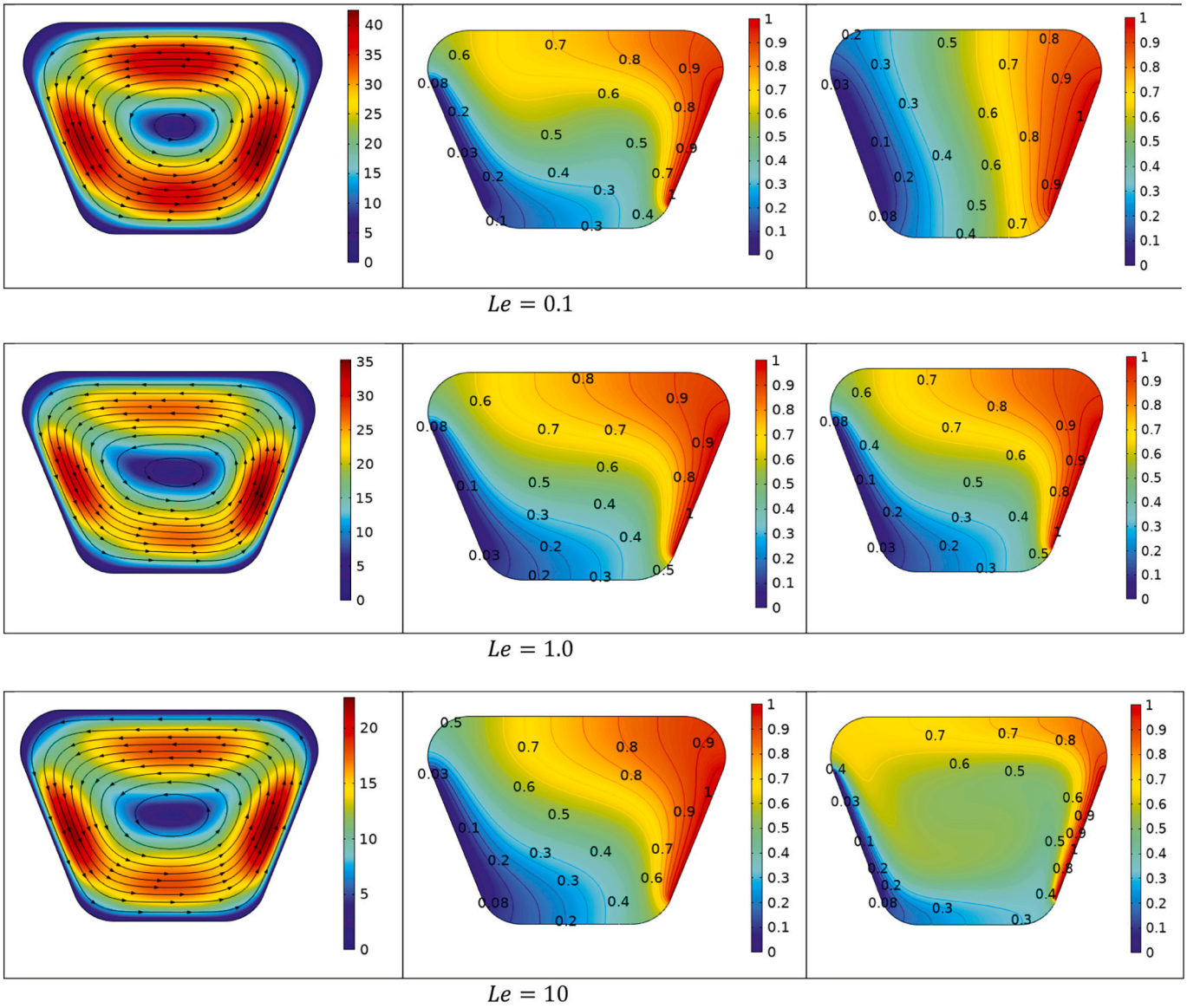

Fig. 4. Variation in velocity, temperature and concentration profile against Lewis number (*Le*).

momentum distribution are observed against (*Le*) because it has no direct relation with momentum diffusivity. The fluid rotates clockwise because of the difference between the temperature of walls at the top and bottom. The results showed that as the Lewis number rises, the fluid concentration near the heated surface rises as well. It's because increasing (*Le*) the thermal diffusion elevates, whereas mass diffusivity declines..

Fig. 5 illustrates the change in velocity, temperature, and concentration distributions versus magnetic field parameter (*Ha*). Since, Hartmann number (*Ha*) is involved in the present study due to the incorporation of the magnetic field, which has a role in reducing velocity profile and making the flow regime laminar. As Hartmann number (*Ha*) shows a ratio of $Ha = BL\sqrt{\frac{\mu}{\sigma}}$ It is observed that the viscosity of fluid enhances against (*Ha*), so temperature distribution decays as well as kinetic energy reduces.

Table 4 represent numerical data regarding a change in the average Nusselt number Nu_{avg} and average Sherwood number (Sh_{avg}) against Hartmann number (*Ha*) and Casson fluid parameter (β) with fixation of $Pr = 6.8$, $Ra = 10^5$, $Le = 2.5$, $N = 1$, $\gamma = 30^o$. It is observed that the mean iNusselt number and Sherwood number occurred the highest for $\beta = 10$ and $Ha = 0$ with magnitudes 2.2759 and 6.6391, respectively. At Ha = 0 there is no magnetic field thus, the resistive forces are absent. Due to this factor, velocity, kinetic energy, and kinetic energy are at the high magnitude, and temperature flux enhances.

Table 5 demonstrates variation in average kinetic energy for the various value of Hartmann number (*Ha*) and Casson parameter (β). It is observed that the kinetic energy at $\beta = 10$ and $Ha = 0$ was increased 10.2 times further than for $\beta = 0.1$ and $Ha = 0$.

Fig. 6 shows the variation of mean Nusselt numbers in different values of iRayleigh and Lewis numbers. For $Pr = 6.8$, $Ha = 25$, $\beta = 1$, $N = 1$ and $\gamma = 30^{\circ}$. As can be seen, the highest mean iNusselt number was obtained at Le = 0.1 and Ra = 107, which is 19.3. Fig. 7 represents a change in the average Sherwood number (Sh_{avg}) against Rayleigh and Lewis numbers with fixation of $Pr = 6.8$, $Ha = 25$, $\beta = 1$, $N = 1$ and $\gamma = 30^{\circ}$. As observed, the average Sherwood number occurred the highest when Le = 10 and $Ra = 10^7$, and it is 30.

5. Concluding remarks

Double Diffusive Natural Convection regime in Casson fluid flow in the trapezoidal enclosure for uniform thermal and concentration

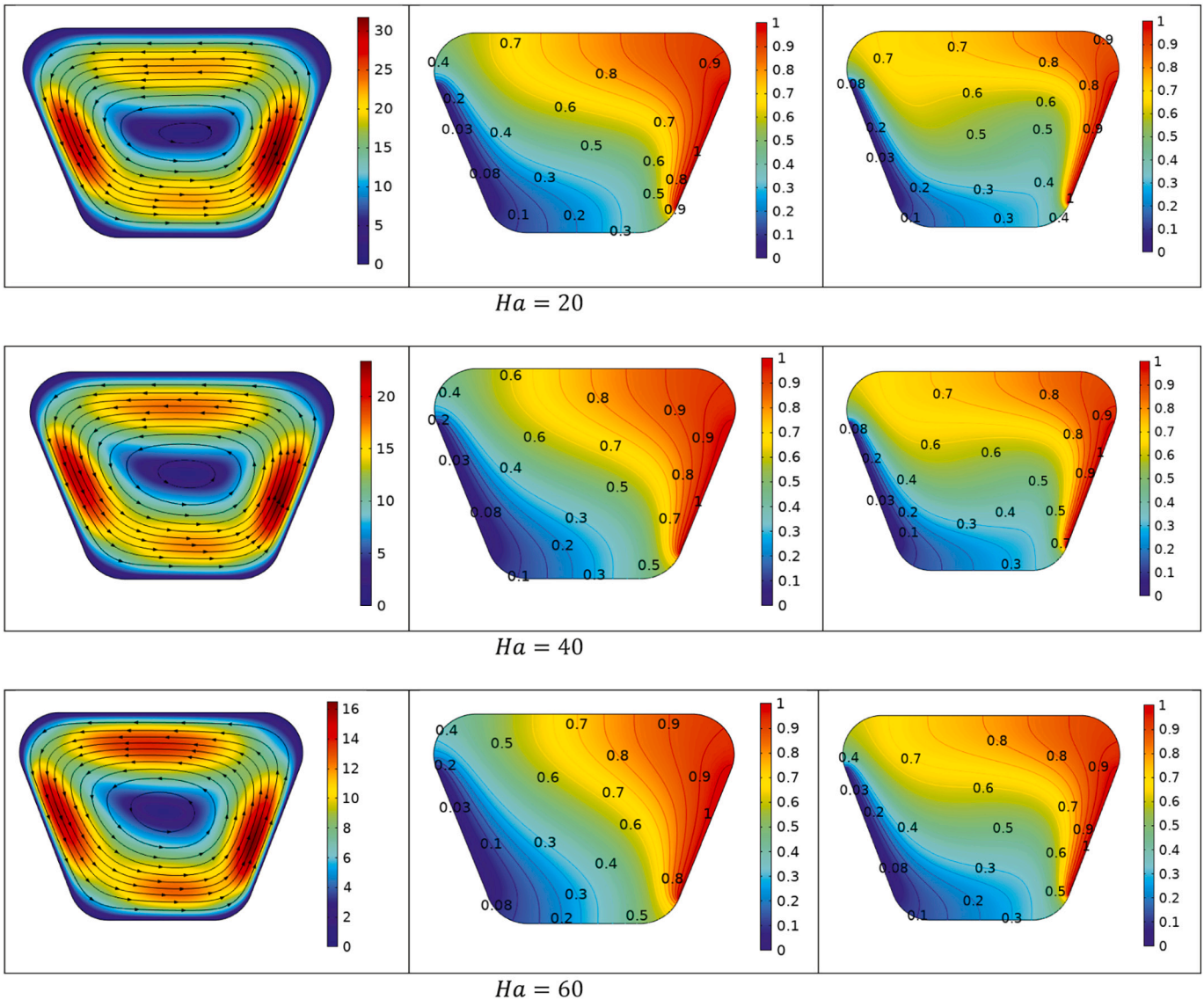

Fig. 5. Variation in velocity, temperature and concentration profile against Hartmann number (*Ha*).

Table 4
Variation of average Nusselt number and Sherwood numbers against Casson parameter (β) and Hartmann number (*Ha*).

Nu_{avg}					Sh_{avg}			
Ha	$\beta = 0.1$	$\beta = 1$	$\beta = 5$	$\beta = 10$	$\beta = 0.1$	$\beta = 1$	$\beta = 5$	$\beta = 10$
0	1.0896	1.8810	2.2149	2.2759	3.2169	5.5786	6.4758	6.6391
25	1.0590	1.6664	1.8852	1.9229	3.1161	5.1757	5.8766	5.9993
50	0.99271	1.3219	1.4153	1.4302	2.8557	4.3159	4.7209	4.7872
75	0.92899	1.0867	1.1245	1.1303	2.5309	3.4468	3.6576	3.6902
100	0.88286	0.95744	0.97363	0.97609	2.2296	2.7676	2.8774	2.8939

Table 5
Variation of kinetic energy against Casson parameter (β) and Hartmann number (*Ha*).

K. E				
Ha	$\beta = 0.1$	$\beta = 1$	$\beta = 5$	$\beta = 10$
0	21.484	129.36	198.84	213.19
25	18.505	84.781	114.49	119.78
50	12.668	37.370	43.668	44.596
75	7.7221	15.904	17.027	17.163
100	4.5102	7.1110	7.2640	7.2797

distributions is analyzed in current communication. Fillets used at the corners of the enclosure to remove singularity formation in the computational domain. A mathematical formulation of a problem by capitalizing on governing law is implemented in the form of a dimensionless system of partial differential equations. Numerical simulations are performed by implementing finite element procedures. Variations in associated momentum, temperature, and concentration distributions in view of steam lines, isothermal and isoconcentration patterns are disclosed. Engineering quantities of interest such that kinetic energy, local heat, and mass flux coefficients is also measured against dimensionless involved physical parameters. Key findings of the current analysis are

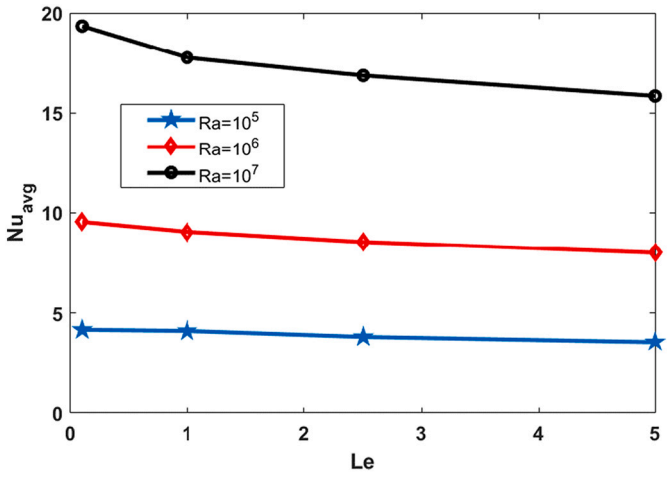

Fig. 6. Variation in average Nusselt number for different values of *Ra* and iLewis number (*Le*) for $Pr = 6.8$, $Ha = 25$, $\beta = 1$, $N = 1$ and $\gamma = 30^{\circ}$.

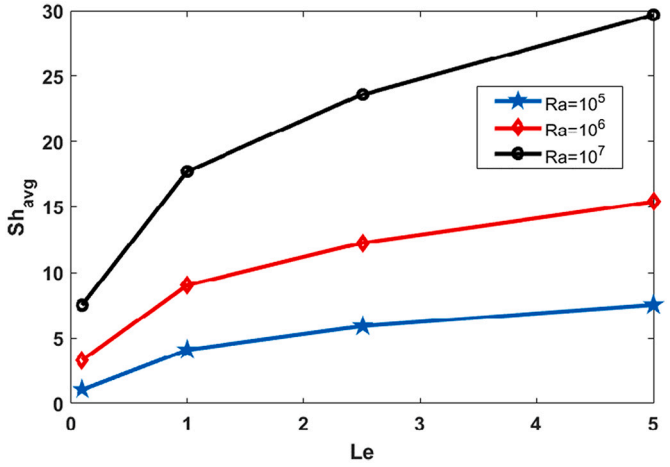

Fig. 7. Variation of average Sherwood number for different values of *Ra* and Lewis number (*Le*) for $Pr = 6.8$, $Ha = 25$, $\beta = 1$, $N = 1$ and $\gamma = 30^{\circ}$.

enlisted below

i) By increasing Lewis number, mass distribution reduces justified by isoconcentration pattern.
ii) Uplift in the magnitude of Rayleigh number (*Ra*) increases the temperature distribution whereas depreciates concentration profile.
iii) The Rayleigh number is a key factor in controlling convection.

Intensification in kinetic energy is revealed against (*Ha*), whereas a contrary attribute is observed against (β).

iv) Heat and mass flux coefficients show diminishing aspects against Hartmann number (*Ha*).
v) Against Casson parameter (β) heat and mass flux distribution show upsurging behavior.

Nomenclature

x & y	Horizontal & vertical coordinate (dimensional) (m/s)
u & *v*	x & y coordinate velocity (dimensional) (m/s)
P	fluid pressure (dimensional) (Pascals)
T	Temperature (dimensional) (Kelvin)
Le	Lewis number
Pr	Prandtl number
g	Gravity (m/s)
Ra	Rayleigh number
DOF	degree of freedom
B	Magnetic field Tesla
c_p	Specific heat ($J.\ kg^{-1}.\ K^{-1}$)
k_e	Thermal conductivity (effective) ($W.\ m^{-1}.\ K^{-1}$)
α_e	Thermal diffusivity (effective) ($m^2.\ sec^{-1}$)
Nu	Nusselt number (local)
c	Concentration (dimensional) (Mass/Volume)
Sh	Sherwood number(local)
NEL	number of elements

Greek symbols

β	Casson fluid parameter
θ	temperature (dimensionless)
ρ	Fluid density ($kg.m^{-3}$)

Credi author statement

Hasan Shahzad: idea and software.
Qurrat Ul Ain: Writing the manuscript.
Imtiaz Ali Shah: arranging the results and collection of data.
Muhammad Bilal Hafeez: review.
Marek Krawczuk: funding.
Abuzar Ghaffari: supervision.

Declaration of Competing Interest

The authors have no conflict of interest to disclose.

Acknowledgments

This project was funded by the Deanship of Scientific Research (DSR), King Abdulaziz University, Jeddah, under grant No. (D-371-135-1443). The authors, therefore, gratefully acknowledge DSR technical and financial support.

References

[1] J.S. Turner, Double diffusive phenomena, Annu. Rev. Fluid Mech. 6 (1974) 37–56.
[2] H.E. Huppert, R.S.J. Sparks, Double-diffusive convection due to crystallization in magmas, Annu. Rev. Earth Planet. Sci. 12 (1984) 11–37.
[3] R.W. Schmitt, Double diffusion in oceanography, Annu. Rev. Fluid Mech. 26 (1994) 255–285.
[4] S. Ostrach, Fluid mechanics in crystal growth–the 1982 freeman scholar lecture, J. Fluids Eng. 105 (1) (1983) 5–20.
[5] R. Viskanta, T.L. Bergman, F.P. Incopera, Double-diffusive natural convection, in: S. Kakac, W. Aung, R. Viskanta (Eds.), Natural Convection: Fundamentals and Applications, Hemisphere, Washington, DC, 1985, pp. 1075–1099.
[6] B. Gebhart, L. Pera, The nature of vertical natural convection flows resulting from the combined buoyancy effects of thermal and mass diffusion, Int. J. Heat Mass Transf. 14 (12) (1971) 2025–2050.
[7] A. Bejan, Mass and heat transfer by natural convection in a vertical cavity, Int. J. Heat Fluid Flow 6 (3) (1985) 149–159.
[8] M. Mobedi, Ü. Özkol, B. Sunden, Visualization of diffusion and convection heat transport in a square cavity with natural convection, Int. J. Heat Mass (2022).
[9] N. Nithyadevi, R. Yang, Double diffusive natural convection in a partially heated enclosure with Soret and Dufour effects, Int. J. Heat Fluid Flow 30 (5) (2009) 902–910.
[10] R. Nikbakhti, A.B. Rahimi, Double-diffusive natural convection in a rectangular cavity with partially thermally active side walls, J. Taiwan Inst. Chem. Eng. 43 (4) (2012) 535–541.
[11] Y.D. Reddy, F. Mebarek-Oudina, B.S. Goud, A.I. Ismail, Radiation, velocity and thermal slips effect toward MHD boundary layer flow through heat and mass transport of Williamson Nanofluid with porous medium, Arab. J. Sci. Eng. (2022), https://doi.org/10.1007/s13369-022-06825-2.
[12] K.K. Asogwa, F. Mebarek-Oudina, I.L. Animasaun, Comparative investigation of water-based Al2O3 nanoparticles through water-based CuO nanoparticles over an exponentially accelerated radiative Riga plate surface via heat transport, Arab. J. Sci. Eng. 123 (2022), https://doi.org/10.1007/s13369-021-06355-3.

[13] F. Mebarek-Oudina, H. Laouira, A.K. Hussein, M. Omri, A. Abderrahmane, L. Kolsi, U. Biswal, Mixed convection inside a duct with an open trapezoidal cavity equipped with two discrete heat sources and moving walls, Mathematics 10 (6) (2022) 1–15, https://doi.org/10.3390/math10060929.
[14] B.V. Pushpa, M. Sankar, F. Mebarek-Oudina, Buoyant convective flow and heat dissipation of cu–H 2 O Nanoliquids in an annulus through a thin baffle, J. Nanofluids 10 (2) (2021) 292–304, https://doi.org/10.1166/jon.2021.1782.
[15] A. Karimdoost Yasuri, M. Izadi, H. Hatami, Numerical study of natural convection in a square enclosure filled by nanofluid with a baffle in the presence of magnetic field, Iran, J. Chem. Chem. Eng. (IJCCE) 38 (2019) 209–220.
[16] B.J. Gireesha, B.M. Shankaralingappa, B.C. Prasannakumar, B. Nagaraja, MHD flow and melting heat transfer of dusty Casson fluid over a stretching sheet with Cattaneo–Christov heat flux model, Int. J. Ambient Energy (2020) 1–9.
[17] M.R. Eid, F. Mabood, Entropy analysis of a hydromagnetic micropolar dusty carbon NTs-kerosene nanofluid with heat generation: Darcy–Forchheimer scheme, J. Therm. Anal. Calorim. 143 (2021) 2419–2436, 2021/02/01.
[18] A.S. Warke, K. Ramesh, F. Mebarek-Oudina, A. Abidi, Numerical investigation of the stagnation point flow of radiative magnetomicropolar liquid past a heated porous stretching sheet, J. Therm. Anal. Calorim. 147 (12) (2022) 6901–6912, https://doi.org/10.1007/s10973-021-10976-z.
[19] I. Chabani, F. Mebarek-Oudina, A.A.I. Ismail, MHD flow of a hybrid Nano-fluid in a triangular enclosure with zigzags and an elliptic obstacle, Micromachines 13 (2) (2022) 1–17, https://doi.org/10.3390/mi13020224.
[20] M. Ferhi, R. Djebali, F. Mebarek-Oudina, N.H. Abu-Hamdeh, S. Abboudi, Magnetohydrodynamic free convection through entropy generation scrutiny of eco-friendly Nanoliquid in a divided L-shaped heat exchanger with lattice Boltzmann method simulation, J. Nanofluids 11 (1) (2022) 99–112, https://doi.org/10.1166/jon.2022.1819.
[21] R. Fares, F. Mebarek-Oudina, A. Aissa, S.M. Bilal, H.F. Öztop, Optimal entropy generation in Darcy-Forchheimer magnetized flow in a square enclosure filled with silver based water nanoliquid, J. Therm. Anal. Calorim. 147 (2) (2022) 1571–1581, https://doi.org/10.1007/s10973-020-10518-z.
[22] A. Hajatzadeh Pordanjani, S. Aghakhani, A. Karimipour, M. Afrand, M. Goodarzi, Investigation of free convection heat transfer and entropy generation of nanofluid flow inside a cavity affected by magnetic field and thermal radiation, J. Therm. Anal. Calorim. 137 (2019) 997–1019, 2019/08/01.
[23] A.H. Mahmoudi, E. Abu-Nada, Combined effect of magnetic field and nanofluid variable properties on heat transfer enhancement in natural convection, Numer. Heat Transf. Part A Appl. 63 (2013) 452–472, 2013/03/15.
[24] M.A. Mansour, M.A. Bakeir, A. Chamkha, Natural convection inside a C-shaped nanofluid-filled enclosure with localized heat sources, Int. J. Numer. Meth. Heat Fluid Flow 24 (2014) 1954–1978, 2014/10/28.
[25] B. Mliki, M.A. Abbassi, K. Guedri, A. Omri, Lattice Boltzmann simulation of natural convection in an L-shaped enclosure in the presence of nanofluid, Eng. Sci. Technol. 18 (2015) 503–511, 2015/09/01/.
[26] O. Turan, A. Sachdeva, N. Chakraborty, R.J. Poole, Laminar natural convection of power-law fluids in a square enclosure with differentially heated side walls subjected to constant temperatures, J. Non-Newton Fluid Mech. 166 (2011) 1049–1063 (CrossRef).
[27] P. Ternik, R. Rudolf, Laminar natural convection of non-Newtonian nanofluid in a square enclosure whit differentially heated side walls, Int. J. Simul. Model. 12 (2013) 5–16 [CrossRef].
[28] A. Sojoudi, S.C. Saha, Y. Gu, M.A. Hossain, Steady natural convection of non-Newtonian power-law fluid in a trapezoidal enclosure, Adv. Mech. Eng. 53 (2013) 653–668 [CrossRef].
[29] O. Turan, A. Sachdeva, R.J. Poole, N. Chakraborty, Aspect ratio and boundary conditions effects on laminar natural convection of power-law fluids in a rectangular enclosure with differentially heated side walls, Int. J. Heat Mass Transf. 60 (2013) 722–738 [CrossRef].
[30] P. Ternik, J. Buchmeister, Buoyacy-induced flow and heat transfer of power law fluids in a side heated square cavity, Int. J. Simul. Model. 14 (2015) 238–249 [CrossRef].
[31] Z. Alloui, P. Vasseur, Natural convection of Carreau–Yasuda non-Newtonian fluids in a vertical cavity heated from the sides, Int. J. Heat Mass Transf. 84 (2015) 912–924 [CrossRef].
[32] S.T. Mohyud-Din, M. Usman, W. Wang, M. Hamid, A study of heat transfer analysis for squeezing flow of a Casson fluid via differential transform method, Neural Comput. & Applic. (2017) 1–2.
[33] S.T. Mohyud-Din, T. Zubair, M. Usman, M. Hamid, M. Rafiq, S. Mohsin, Investigation of heat and mass transfer under the influence of variable diffusion coefficient and thermal conductivity, Ind. J. Phys. (2018) 1–9.
[34] A. Hussanan, M.Z. Salleh, I. Khan, S. Shafie, Analytical solution for suction and injection flow of a viscoplastic Casson fluid past a stretching surface in the presence of viscous dissipation, Neural Comput. & Applic. 29 (12) (2018) 1507–1515.
[35] G.J. Reddy, B. Kethireddy, M. Kumar, M.M. Hoque, A molecular dynamics study on transient non-Newtonian MHD Casson fluid flow dispersion over a radiative vertical cylinder with entropy heat generation, J. Mol. Liq. 252 (2018) 245–262.
[36] M. Hamid, M. Usman, Z.H. Khan, R. Ahmad, W. Wang, Dual solutions and stability analysis of flow and heat transfer of Casson fluid over the stretching sheet, Phys. Lett. A 383 (20) (2019) 2400–2408.
[37] M. Goodarzi, M.R. Safaei, A. Karimipour, K. Hooman, M. Dahari, S.N. Kazi, et al., Comparison of the finite volume and lattice Boltzmann methods for solving natural convection heat transfer problems inside cavities and enclosures, Abstr. Appl. Anal. 762184 (2014), 2014/02/09.
[38] S. Hussain, F. Schieweck, S. Turek, Efficient Newton multigrid solution techniques for higher order space time Galerkin discretizations of incompressible flow, Appl. Numer. Math. 83 (2014) 51–71.
[39] S. Hussain, S. Shoeibi, Taher Armaghani, impact of magnetic field and entropy generation of Casson fluid on double diffusive natural convection in staggered cavity, Int. Comm. Heat Mass Transf. 127 (2021), 105520.